nature materials

ARTICLES

PUBLISHED ONLINE: 13 JUNE 2016 | DOI: 10.1038/NMAT4660

The role of electronic coupling between substrate and 2D MoS_2 nanosheets in electrocatalytic production of hydrogen

Damien Voiry[1], Raymond Fullon[1], Jieun Yang[1], Cecilia de Carvalho Castro e Silva[1], Rajesh Kappera[1], Ibrahim Bozkurt[1], Daniel Kaplan[2], Maureen J. Lagos[1,3,4], Philip E. Batson[1,3,4], Gautam Gupta[5], Aditya D. Mohite[5], Liang Dong[6], Dequan Er[6], Vivek B. Shenoy[6], Tewodros Asefa[7,8] and Manish Chhowalla[1]*

The excellent catalytic activity of metallic MoS_2 edges for the hydrogen evolution reaction (HER) has led to substantial efforts towards increasing the edge concentration. The 2H basal plane is less active for the HER because it is less conducting and therefore possesses less efficient charge transfer kinetics. Here we show that the activity of the 2H basal planes of monolayer MoS_2 nanosheets can be made comparable to state-of-the-art catalytic properties of metallic edges and the 1T phase by improving the electrical coupling between the substrate and the catalyst so that electron injection from the electrode and transport to the catalyst active site is facilitated. Phase-engineered low-resistance contacts on monolayer 2H-phase MoS_2 basal plane lead to higher efficiency of charge injection in the nanosheets so that its intrinsic activity towards the HER can be measured. We demonstrate that onset potentials and Tafel slopes of ~−0.1 V and ~50 mV per decade can be achieved from 2H-phase catalysts where only the basal plane is exposed. We show that efficient charge injection and the presence of naturally occurring sulfur vacancies are responsible for the observed increase in catalytic activity of the 2H basal plane. Our results provide new insights into the role of contact resistance and charge transport on the performance of two-dimensional MoS_2 nanosheet catalysts for the HER.

The development of catalysts from earth-abundant and inexpensive materials is essential for the implementation of clean energy technologies using hydrogen[1–4]. Transition metal dichalcogenides such as MoS_2 and WS_2 have emerged as promising catalysts for the hydrogen evolution reaction (HER) in acidic media[5–8]. Substantial work has been devoted to understanding and optimizing the catalytic properties of these materials[9–16]. Pioneering work by Jaramillo *et al.*[10] has shown that it is the metallic edges of ultrahigh-vacuum-grown MoS_2 nanoclusters that are catalytically active whereas the less conducting 2H basal plane remains relatively inactive. Numerous follow-up studies have demonstrated that increasing the concentration of exposed edges can lead to improvements in catalytic performance[17–20]. Recent work has suggested that enhancing the conductivity of the basal plane by phase transformation from the semiconducting 2H phase to the metallic 1T phase also leads to an improvement in performance[7,13,14,21,22]. In the case of 1T-phase MoS_2 and WS_2, the catalytic properties seem to be independent of the edges and primarily dependent on the concentration of the metallic phase[7,13,22]. Theoretical studies have suggested that, for the same catalyst, it is possible to improve the catalytic performance by enhancing the coupling between the substrate and the active material to decrease the energy of hydrogen adsorption[23]. In addition, the role of electrical coupling between the substrate and catalysts on the cathode and resulting charge transfer kinetics has also been reported to be important[21,22,24,25]. Thus, facilitating charge transfer through engineering better electrical contacts between the support and catalyst nanoparticles is an additional important variable.

In electrocatalysis, the substrate supports the catalyst material and injects or collects charge carriers from the electrocatalyst. Here, to estimate the contact resistance of individual catalyst nanosheets, the supporting substrate cannot be conducting. We used SiO_2 on Si wafers. The gold contacts deposited on the MoS_2 nanosheets are therefore the electrical contacts and thus act as conducting substrates. We demonstrate that the basal plane of the 2H phase can be as catalytically active as the edges or the 1T phase. A key parameter in increasing the catalytic activity of the 2H basal plane is the enhancement of the charge transfer from the substrate to the catalyst active sites by reducing the contact resistance and improving the conductivity of the catalyst. To demonstrate this, we have carried out a study to understand the role of edges, phases, doping and electrical coupling (or the contact resistance) on the catalytic properties by measuring the HER performance of individual monolayers of chemical vapour deposited MoS_2 nanosheets

[1]Materials Science and Engineering, Rutgers University, 607 Taylor Road, Piscataway, New Jersey 08854, USA. [2]US Army RDECOM-ARDEC, Acoustics and Networked Sensors Division, Picatinny Arsenal, New Jersey 07806, USA. [3]Department of Physics, Rutgers University, 136 Frelinghuysen Road, New Jersey 08854, USA. [4]Institute for Advanced Materials, Devices and Nanotechnology, Rutgers University, 607 Taylor Road, New Jersey 08854, USA. [5]MPA-11 Materials Synthesis and Integrated Devices, Los Alamos National Laboratory, Los Alamos, New Mexico 87545, USA. [6]Department of Materials Science and Engineering, University of Pennsylvania, Philadelphia, Pennsylvania 19104, USA. [7]Department of Chemistry and Chemical Biology, Rutgers University, 610 Taylor Road, Piscataway, New Jersey 08854, USA. [8]Department of Chemical and Biochemical Engineering, Rutgers University, 98 Brett Road, Piscataway, New Jersey 08854, USA. *e-mail: manish1@rci.rutgers.edu

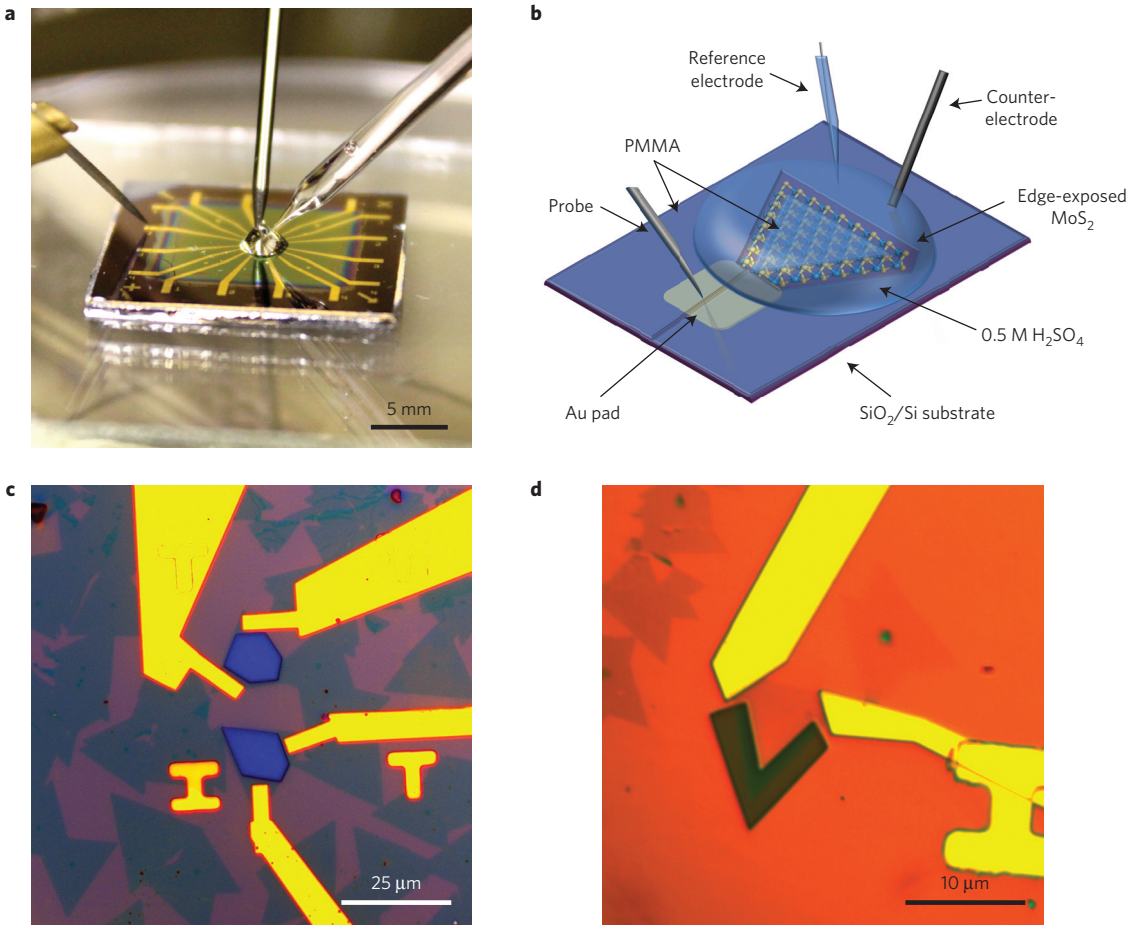

Figure 1 | Electrochemical set-up for the HER measurement on single-layer MoS_2. a, Photograph of the electrochemical microcell. **b**, Schematic of the set-up showing single layer of MoS_2 deposited on SiO_2 and contacted by one gold electrode. Glassy carbon and Ag/AgCl electrodes are used as counter and reference electrode, respectively. The entire substrate is covered with poly(methylmethacrylate) PMMA, with the exception of a window on top of the edges of the MoS_2 nanosheet. Only the MoS_2 nanosheet is in contact with the electrolyte solution (0.5 M H_2SO_4). Edge-exposed and edge-covered cells can be fabricated and tested. **c**,**d**, Optical microscope images of the different types of microcells: CVD-grown single-layer MoS_2 having their edge covered (**c**) or exposed (**d**). Such cells enable one to control precisely the quantity of MoS_2 sites exposed and thus an accurate estimation of the number of turnovers at each active site.

(see Supplementary Information and Methods). We have developed an experimental set-up to measure the catalytic activity of individual nanosheets of MoS_2, as shown in Fig. 1a,b. By using electron beam lithography patterning (Supplementary Fig. 2), we have been able to measure the catalytic properties of only the basal plane (while covering the edges, Fig. 1c) or only the edges (while covering the basal plane, Fig. 1d). The devices in Fig. 1c,d are top-contacted, but bottom-contacted devices were also tested. The electrical properties of top- and bottom-contacted devices are similar, suggesting that the charge injection mechanism in both cases is the same. In addition, we have been able to engineer the phases to compare the catalytic performance of the metallic and semiconducting phases. The catalytic properties of the individual monolayer MoS_2 nanosheets were measured using a three-electrode configuration, with glassy carbon as the counter-electrode, Ag/AgCl electrode as the reference electrode, and one gold pad contacting the single-layer MoS_2 nanosheet as the working electrode. Everything except the MoS_2 was covered with cured poly(methylmethacrylate) (PMMA) resist to ensure that the measured activity was due to the MoS_2 only.

The deposition of metals such as gold directly on top of ultrathin or monolayer semiconducting 2H-phase MoS_2 leads to Schottky contacts (energy barrier of ~0.2 eV; refs 26–29) that are responsible for the observed high contact resistance[26,28,30–33]. Furthermore, it is not possible to vary the Schottky barrier height in MoS_2 by using metals of different work functions owing to the Fermi level pinning effect[34]. The contact resistance is also variable, so that values ranging from 1 to 10^6 kΩ mm are possible[33]. However, contact resistance values lower than 1 kΩ mm are difficult to achieve on 2H-phase MoS_2. In contrast, it is generally difficult to make high-resistance contacts on the 1T phase of MoS_2 (refs 35,36). Thus, the range of contact resistances we obtain for the 1T phase is narrower (between 10^{-5} and 10^{-2} kΩ mm) than for the 2H phase (1–10^6 kΩ mm). The lower contact resistances in the 1T-phase devices are translated into superior HER catalytic performance[13,21,22].

To differentiate between the contribution of the contacts and the internal resistance of the measurement system, impedance spectroscopy was performed on MoS_2 microcells with varying contact resistances. In electrochemistry, the contact resistance is often subtracted from the measured signal in order to eliminate its influence on the electrochemical performance of the material being tested. This assumes that the contact resistance does not play a significant role in determining the measured catalytic properties. However, we demonstrate that in the case of basal plane of MoS_2, existing catalytic sites are not active at high contact resistance values but can be activated by decreasing the contact resistance to facilitate charge injection. Here, the contact resistance is a variable that we can independently control in our devices, which allows us to investigate the role of charge injection on the catalytic

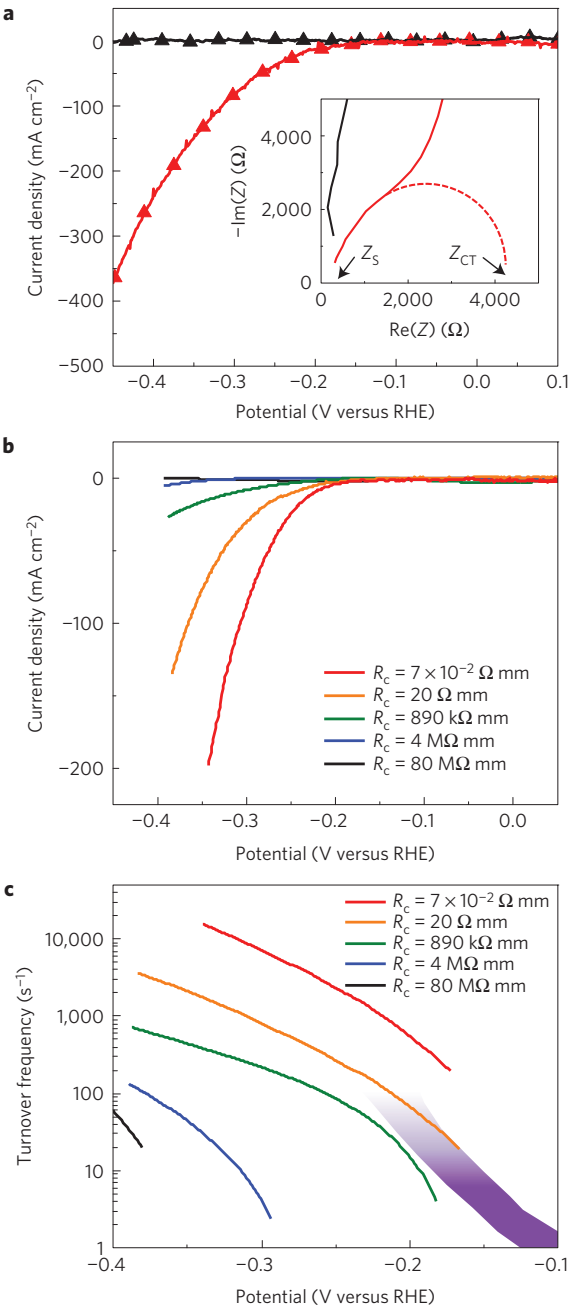

Figure 2 | Electrochemical measurements from individual single-layer MoS_2 nanosheets. a, Polarization curves measured from two MoS_2 microcells with (solid line) and without iR correction (triangles). Polarization curves from MoS_2 microcells with low and high contact resistance are shown in red and black, respectively. Inset: corresponding Nyquist plots showing that the internal resistance (Z_S) ~ 300 Ω does not vary with the contact resistance. The charge transfer resistance (Z_{CT}) is strongly governed by the contact resistance. For the best contact resistance, Z_{CT} ~ 4,000 Ω can be measured. **b**, Polarization curves obtained from MoS_2 devices with various contact resistances from 80 MΩ mm down to 7×10^{-2} Ω mm. The performance of the MoS_2 devices increases rapidly with decreasing contact resistance. **c**, Evolution of the turnover frequency (TOF) with the overpotential. The TOF values are calculated from the polarization curves presented in **a** (see Supplementary Methods). The quantity of active sites has been estimated assuming that the entire surface of MoS_2 (that is, surface and edge sites) is active. The TOF values are compared to the values obtained from metallic 2H-phase MoS_2 edges grown on gold from ref. 10 (purple region).

performance. We have recently demonstrated that it is possible to locally engineer the contact resistance by phase engineering[35,36]. That is, locally transforming the 2H phase to the metallic 1T phase and depositing the metal electrode directly on top of the 1T phase allows the realization of low-resistance contacts that are strongly electrically coupled to the 2H phase[35]. We have used this technique to successfully reduce the contact resistance in field-effect transistors[35,36]. Furthermore, we have shown that the interface between the patterned 1T phase and the 2H phase is atomically sharp[37]. Typical Nyquist plots obtained from single MoS_2 nanosheets with high and low contact resistances are presented in Fig. 2a. The internal resistance remains relatively small (Z_S ~ 300 Ω) and does not depend on the contact resistance between the MoS_2 and the gold electrode (inset Fig. 2a). The contribution of the internal resistance on the polarization curve remains low, and thus correction of the iR drop is negligible (Fig. 2a). However, the influence of contact resistance can be observed from the marked decrease of the charge transfer resistance (Z_{CT}) in the Nyquist plots (inset Fig. 2a), consistent with results from the literature[21,22,24,25,38]. For high contact resistance, the charge transfer resistance (Z_{CT}), which represents the efficiency of the electron transfer between the gold pads and the MoS_2 nanosheets, becomes virtually infinite. At low contact resistance, the Z_{CT} reduces significantly and reaches ~4,000 Ω, suggesting a large improvement in the efficiency of the electron transfer between gold and MoS_2 (inset Fig. 2a).

The polarization curves of the current density for various contact resistances (see Supplementary Information for calculations of contact resistance) in 0.5 M H_2SO_4 are shown in Fig. 2b. The measurements in Fig. 2b are averages taken from the 2H and 1T phase, and from the basal plane and edges of numerous samples. It can be seen that the HER performance increases with a decrease in contact resistance, irrespective of whether the edges or basal plane are exposed. The current densities reported here are from flat MoS_2 electrodes, and therefore slightly lower than the high-surface-area mesoscopic electrodes reported in the literature[19,21,38,39]. Electrocatalysis from monolayer MoS_2 allows accurate measurement of the surface exposed to the electrolyte, which can be used to calculate the turnover frequency (TOF), an indicator of the activity of the catalytic sites. The TOF values reported in the literature remain virtually the same[20], suggesting that the improvement of the electrodes is essentially coming from an increase in the number of active sites and not from an increase in the intrinsic activity of each site. The evolution of the TOF (in s^{-1}) with applied potential for several contact resistances is shown in Fig. 2c. As expected, the TOF values increase with overpotential. For the low-contact-resistance devices, we obtain TOFs of $>100\,s^{-1}$ and $>1{,}000\,s^{-1}$ at overpotentials of 200 mV and 300 mV, respectively. These values compare favourably with other reports based on MoS_2 catalysts (Supplementary Fig. 8)[20]. For the lowest contact resistance, the activity of the MoS_2 nanosheets is higher than directly grown MoS_2 clusters on gold reported by Jaramillo *et al.*[10], as shown in Fig. 2c.

The variation of the onset potential and the Tafel slopes with contact resistances are summarized in Fig. 3a,b, respectively, while the current densities (at $\eta = 400$ mV) are shown in Fig. 3c. It can be seen that for low-resistance contacts, exceptionally low onset potential <0.15 V and Tafel slopes as low as ~45 mV per decade can be obtained for the best electrodes (Fig. 3a,b). Figure 3b,c also reveals that below a critical resistance value of ~10–100 kΩ mm, the Tafel slope and current density essentially saturate at ~60 mV per decade and 100 mA cm^{-2}. It can also be seen from Fig. 3b,c that it is possible to obtain similar HER performance in the 2H phase where the edges are covered and therefore do not contribute to the reaction. This shows that the basal plane of the 2H phase, which has been previously thought to be less catalytically active, exhibits HER properties that are consistent with what has been reported in the literature for edges and the 1T phase[19–22] by improving the electrical

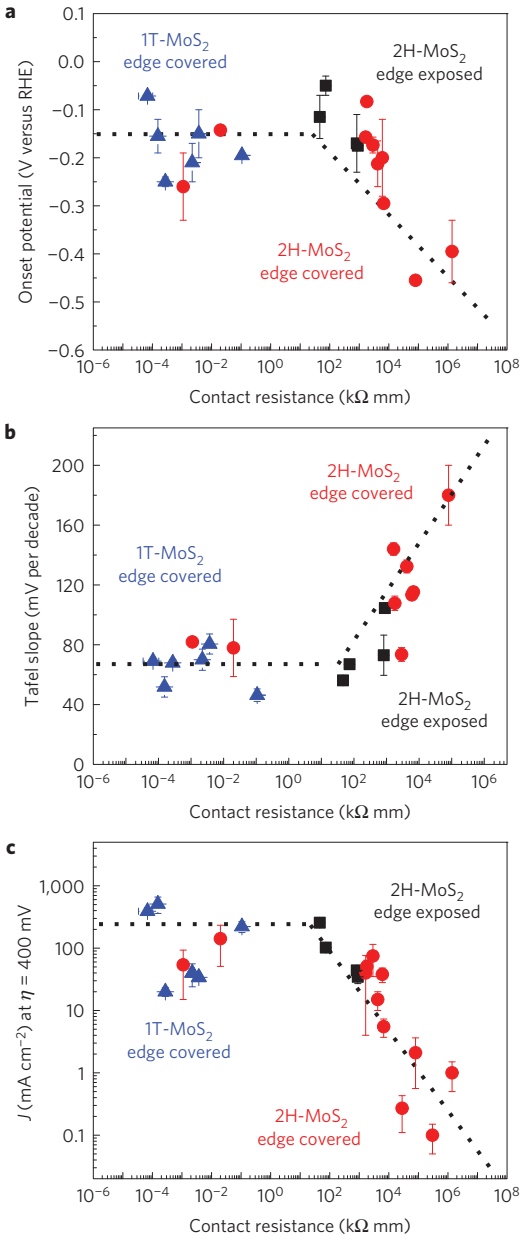

Figure 3 | Influence of the contact resistance on the HER performances of MoS_2. a–c, Variation of the onset potential (**a**), Tafel slope values (**b**) and current density (**c**) measured at $\eta = 400$ mV with the contact resistance (R_c). The HER activity of the MoS_2 electrodes is progressively enhanced as the contact resistance decreases. For $R_c < 10$ kΩ mm, the MoS_2 activity stabilizes and current density of >100 mA cm^{-2} at $\eta = 400$ mV can be obtained from the MoS_2 basal planes. No significant differences between edge-exposed and edge-covered devices have been observed from the samples, suggesting that both the surface and the edges of the MoS_2 crystals are active.

coupling (or reducing the contact resistance) between the substrate and the catalyst.

It is possible to obtain low-resistance contacts in devices where the 2H basal plane is exposed to electrolyte (see 'Preparation of 2H-phase MoS_2 electrochemical microcells with 1T-phase contacts' in Supplementary Information). From Fig. 3, it can be seen that for low-contact-resistance (~10^{-2} kΩ mm) devices where only the 2H-phase MoS_2 basal plane is exposed, the HER performance is indeed comparable to that of 1T-phase and edge-exposed devices. Thus, our results suggest that the catalytic activity of the basal plane and edges of CVD MoS_2, irrespective of the phases, is comparable. This is not surprising because the structures of the 1T and 2H phases of MoS_2 are comparable (Supplementary Fig. 11). However, in the case of 2H-phase MoS_2, the typically high contact resistance limits the Volmer reaction: $H_3O^+ + e^- \rightarrow H_{ads} + H_2O$, which requires efficient charge transfer[40]. That is, if the catalyst material is not sufficiently conducting, then electron transport to the active sites is limited, preventing the Volmer reaction from proceeding. This is indeed demonstrated in Fig. 3b, where the Tafel slope values range from ~40 to 50 mV per decade for the lowest contact resistance and up to ~120 mV per decade or higher for the highest values of contact resistance. Tafel slopes of ~40 mV per decade suggest a Volmer–Heyrovsky mechanism at the surface of MoS_2 with the hydrogen desorption reaction: $H_{ads} + H_3O^+ + e^- \rightarrow H_2 + H_2O$ as the limiting step[7,21,22,24]. Our HER measurements on single MoS_2 nanosheets demonstrate that the mechanism for hydrogen evolution is markedly influenced by the efficiency of electron injection from the substrate to the catalyst and its transport to the active site. Tafel slopes of 120 mV per decade correspond to a mechanism where the hydrogen adsorption (Volmer reaction) is the limiting reaction. This is the case when the energy of hydrogen adsorption is high, making the process inefficient. This is expected here for the high contact resistance values because hydrogen adsorption cannot be favourable in the absence of electrons at the active sites owing to the poor electrical conductance of the catalyst (Fig. 3b). On the other hand, improved electrical coupling enables the hydrogen to adsorb easily on MoS_2 and the reaction process through the Volmer–Heyrovsky mechanism, as observed in the present study and for metallic 1T-phase MoS_2 or MoS_2 grown on conducting reduced graphene oxide[14,21,22,24].

The basal plane activity of 2H-phase MoS_2 observed in our work is in contrast with the literature[9,10,19]. The activity of 2H-phase MoS_2 basal planes is expected to be significantly lower than edges owing to the lower energy of hydrogen adsorption (ΔG_{H^*}) at the edge sites[7,9,10]. To confirm the 2H-phase basal plane activity, we examined the HER activity from single-layer MoS_2 nanosheets on glassy carbon with contact resistance <100 kΩ mm (see 'Edges versus basal planes for SL 2H-phase MoS_2' in Supplementary Information). We found that the basal planes are indeed active towards the evolution of hydrogen, with an exchange current density of 7–16 μA cm^{-2} and a TOF at 0 V of 0.019–0.046 s^{-1}, which is comparable with the previous measurements from MoS_2 nanoclusters grown on gold (Supplementary Table 2)[10]. We attribute the catalytic activity of CVD MoS_2 nanosheets to sulfur vacancies. In a recent contribution, the Zheng and Norskov groups have shown that basal planes of 2H-phase MoS_2 can be activated by increasing the number of single S vacancies and the application of tensile strain on the nanosheets[41]. Defect densities as low as ~3% were predicted to lower ΔG_{H^*} from 2 eV down to 0.2 eV. In the absence of strain, thermo-neutral H adsorption on the surface of 2H-phase MoS_2 would require a density of S vacancies of ~14% (ref. 41). Defects in CVD-grown MoS_2 have been reported by several groups[42–44], and are known to induce pronounced modifications of the electronic and optoelectronic properties[45–47]. Direct observations of these defects can be achieved through high-angle annular dark-field scanning electron microscopy (HAADF-STEM) owing to the contrast obtained by the presence and the nature of the atoms under the electron beam as shown in Fig. 4a,b (ref. 43,44). STEM observations of the MoS_2 nanosheets reveal that defects are naturally present in the samples. Several types of defects have already been reported—such as single S vacancies, double S vacancies, Mo vacancies and Mo–S_x vacancies or antisite defects—and depend strongly on the synthesis methods[43,44]. Careful analysis of the MoS_2 basal plane (>500 nm^2) reveals that the large majority of the defects consist of single S vacancies with a density of the defects of up to ~9% (Fig. 4c), which suggests that the basal

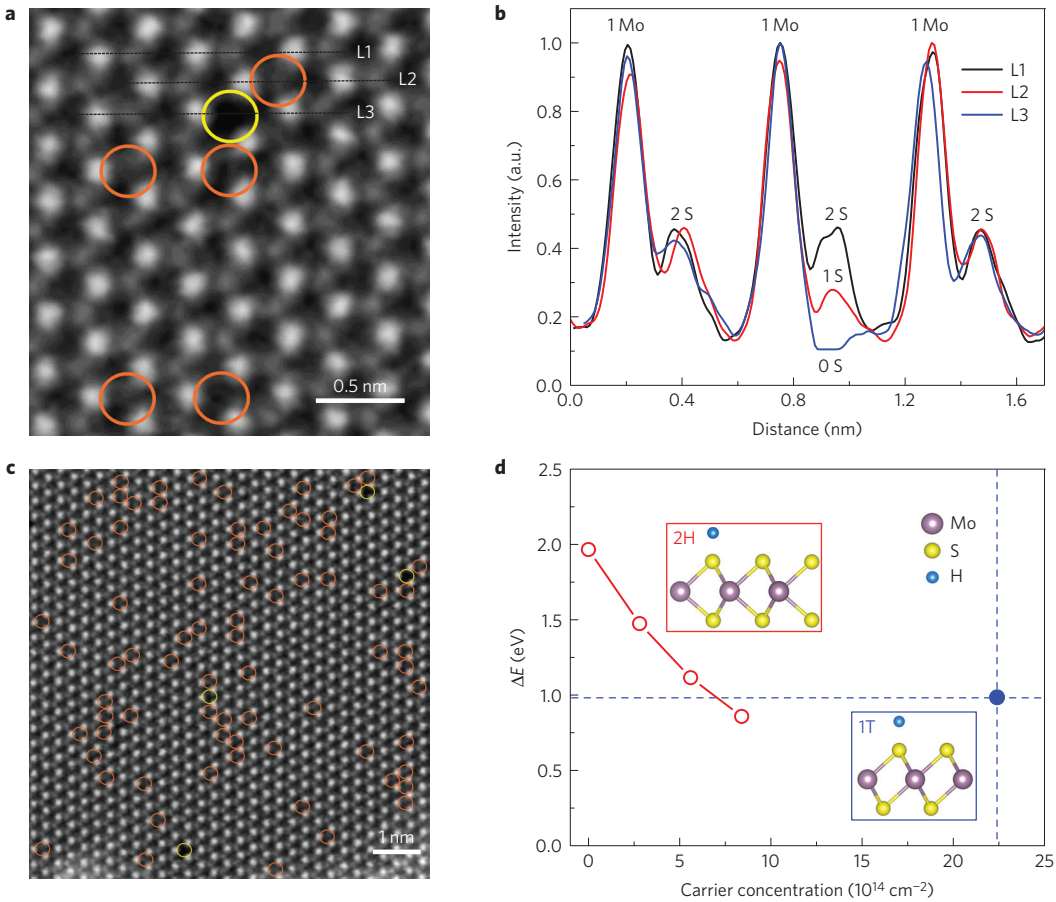

Figure 4 | HAADF-STEM observations of sulfur vacancies in single-layer MoS_2 nanosheets. a, STEM image of a single-layer CVD-grown MoS_2 nanosheet showing different types of defects: single sulfur vacancy (orange circles) and double sulfur vacancy (yellow circles). **b**, Intensity profiles along lines L1–L3. Higher contrast is obtained from the Mo atoms compared to one sulfur atom (~30% of the Mo intensity) and two sulfur atoms (~45% of the Mo intensity). In absence of sulfur atoms (L3), the intensity decreases to <10%. **c**, STEM image of a large-area single-layer MoS_2 nanosheet. The vast majority of the defects are formed by single sulfur vacancies. **d**, The differential hydrogen adsorption energy (ΔE) in 2H-phase MoS_2 decreases significantly with an increased carrier concentration. When the carrier concentration approaches 7×10^{14} cm^{-2}, ΔE in 2H-phase MoS_2 is close to that in the 1T phase.

plane may be activated by the presence of S vacancies[41]. Assuming a density of defects of 9%, the TOF at 0 V from single-layer MoS_2 reaches 0.2–0.5 s^{-1}, in good agreement with the values reported by Li *et al.*: 0.1–0.15 s^{-1} (ref. 41). Thus, our results suggest that low contact resistance can activate sites from the basal plane of MoS_2, probably located at the sulfur vacancies.

Dopants play two important roles in the HER. First, excess electrons lower the Schottky barrier at the contacts so that charge transfer kinetics between the conducting substrate and the MoS_2 nanosheets is substantially improved. This strategy has been widely used in the semiconductor industry to produce ohmic contacts for state-of-the-art electronics. Second, the presence of additional electrons in the MoS_2 lattice significantly decreases the energy of hydrogen adsorption, the first step in the HER, as shown by our density functional theory (DFT) calculations in Fig. 4d. Sulfur vacancies in MoS_2 act as n-type dopants, increasing the density of states at the Fermi level[43–45]. Figure 4d shows the variation of the energy of hydrogen adsorption (ΔE) on the 2H phase of the MoS_2 basal plane at doping carrier concentrations of 0 cm^{-2}, 2.8×10^{14} cm^{-2}, 5.6×10^{14} cm^{-2} and 8.4×10^{14} cm^{-2} and compared to the 1T phase (see details of the calculations in Supplementary Information). It can be seen that ΔE decreases quasi-linearly with the carrier (electron) concentration, suggesting that the ability for the 2H-phase basal planes to adsorb hydrogen improves for a higher concentration of dopants. Using a linear interpolation in Fig. 4d, we estimate that ΔE for 2H-phase MoS_2 becomes lower than in the case of 1T-phase MoS_2 when the carrier concentration reaches 7.3×10^{14} cm^{-2}, consistent with carrier concentrations calculated for 9% S vacancies (see 'Turnover frequency calculations' in Supplementary Information).

A combination of STEM and electrochemical measurements along with our calculations point to unsaturated Mo atoms at sulfur vacancies as the active sites for the HER. These unsaturated sites are similar to the edge sites of MoS_2 that are already known to be highly active towards the HER[9,10]. In a recent report, Tran *et al.* have identified the formation of metal hydrides from unsaturated Mo atoms as a key step in the HER mechanism from amorphous MoS_x (ref. 48). Our results provide additional insight into the origin of HER activity of molybdenum sulfide catalysts and suggest that amorphous MoS_x and MoS_2 nanosheets share a similar mechanism involving unsaturated Mo active sites.

Our work provides new insights into the role of electrical coupling between single-layer MoS_2 nanosheet catalysts and the substrate on the HER catalytic activity. The results show that the basal plane of the 2H-phase MoS_2, previously thought to be catalytically inactive, can exhibit excellent catalytic activity. That is, the basal plane of the MoS_2 surface contains active sites in the form of S vacancies but is rendered inactive for the HER because of the high contact resistance between the catalyst and the support. Our results show that lowering the contact resistance to facilitate charge injection from the substrate to the catalysts leads to realization of the intrinsic catalytic properties of the 2H basal plane. High contact

resistance acts as a severe choke for electron injection to active sites, which limits catalytic activity, especially in the case of the 2H basal plane. For non-metal catalysts, contact resistance is an important variable because of the formation of non-ohmic contacts, which has been widely overlooked until now. Numerous studies have reported the catalytic performance of a wide range of MoS_2 catalysts, but very few explicitly mention the resistance between the catalyst and support. The contact resistance is an essential parameter that must be known to compare the relative performance of different types of MoS_2 catalysts for the HER. We believe these results will provide new directions for the design of large-area electrodes with low contact resistance that could ultimately exploit the full potential of MoS_2 nanosheets for the evolution of hydrogen.

Methods

Methods and any associated references are available in the online version of the paper.

Received 21 January 2016; accepted 3 May 2016; published online 13 June 2016

References

1. Crabtree, G. W., Dresselhaus, M. S. & Buchanan, M. V. The hydrogen economy. *Phys. Today* **57,** 39–44 (December, 2004).
2. Greeley, J., Jaramillo, T. F., Bonde, J., Chorkendorff, I. & Nørskov, J. K. Computational high-throughput screening of electrocatalytic materials for hydrogen evolution. *Nature Mater.* **5,** 909–913 (2006).
3. Vesborg, P. C. K., Seger, B. & Chorkendorff, I. Recent development in hydrogen evolution reaction catalysts and their practical implementation. *J. Phys. Chem. Lett.* **6,** 951–957 (2015).
4. Morales-Guio, C. G., Stern, L.-A. & Hu, X. Nanostructured hydrotreating catalysts for electrochemical hydrogen evolution. *Chem. Soc. Rev.* **43,** 6555–6569 (2014).
5. Yan, Y., Xia, B., Xu, Z. & Wang, X. Recent development of molybdenum sulfides as advanced electrocatalysts for hydrogen evolution reaction. *ACS Catal.* **4,** 1693–1705 (2014).
6. Yang, J. & Shin, H. S. Recent advances in layered transition metal dichalcogenides for hydrogen evolution reaction. *J. Mater. Chem. A* **2,** 5979–5985 (2014).
7. Tsai, C., Chan, K., Nørskov, J. K. & Abild-Pedersen, F. Theoretical insights into the hydrogen evolution activity of layered transition metal dichalcogenides. *Surf. Sci.* **640,** 133–140 (2015).
8. Merki, D. & Hu, X. Recent developments of molybdenum and tungsten sulfides as hydrogen evolution catalysts. *Energy Environ. Sci.* **4,** 3878–3888 (2011).
9. Hinnemann, B. *et al*. Biomimetic hydrogen evolution: MoS_2 nanoparticles as catalyst for hydrogen evolution. *J. Am. Chem. Soc.* **127,** 5308–5309 (2005).
10. Jaramillo, T. F. *et al*. Identification of active edge sites for electrochemical H_2 evolution from MoS_2 nanocatalysts. *Science* **317,** 100–102 (2007).
11. Bonde, J., Moses, P. G., Jaramillo, T. F., Nørskov, J. K. & Chorkendorff, I. Hydrogen evolution on nano-particulate transition metal sulfides. *Faraday Discuss.* **140,** 219–231 (2008).
12. Xie, J. *et al*. Controllable disorder engineering in oxygen-incorporated MoS_2 ultrathin nanosheets for efficient hydrogen evolution. *J. Am. Chem. Soc.* **135,** 17881–17888 (2013).
13. Voiry, D. *et al*. Enhanced catalytic activity in strained chemically exfoliated WS_2 nanosheets for hydrogen evolution. *Nature Mater.* **12,** 850–855 (2013).
14. Wang, H. *et al*. Electrochemical tuning of vertically aligned MoS_2 nanofilms and its application in improving hydrogen evolution reaction. *Proc. Natl Acad. Sci. USA* **110,** 19701–19706 (2013).
15. Merki, D., Vrubel, H., Rovelli, L., Fierro, S. & Hu, X. Fe, Co, and Ni ions promote the catalytic activity of amorphous molybdenum sulfide films for hydrogen evolution. *Chem. Sci.* **3,** 2515–2525 (2012).
16. Merki, D., Fierro, S., Vrubel, H. & Hu, X. Amorphous molybdenum sulfide films as catalysts for electrochemical hydrogen production in water. *Chem. Sci.* **2,** 1262–1267 (2011).
17. Jaramillo, T. F. *et al*. Hydrogen evolution on supported incomplete cubane-type $[Mo_3S_4]^{4+}$ electrocatalysts. *J. Phys. Chem. C* **112,** 17492–17498 (2008).
18. Chen, Z. *et al*. Core–shell MoO_3–MoS_2 nanowires for hydrogen evolution: a functional design for electrocatalytic materials. *Nano Lett.* **11,** 4168–4175 (2011).
19. Kibsgaard, J., Chen, Z., Reinecke, B. N. & Jaramillo, T. F. Engineering the surface structure of MoS_2 to preferentially expose active edge sites for electrocatalysis. *Nature Mater.* **11,** 963–969 (2012).
20. Kibsgaard, J., Jaramillo, T. F. & Besenbacher, F. Building an appropriate active-site motif into a hydrogen-evolution catalyst with thiomolybdate $[Mo_3S_{13}]^{2-}$ clusters. *Nature Chem.* **6,** 248–253 (2014).
21. Lukowski, M. A. *et al*. Enhanced hydrogen evolution catalysis from chemically exfoliated metallic MoS_2 nanosheets. *J. Am. Chem. Soc.* **135,** 10274–10277 (2013).
22. Voiry, D. *et al*. Conducting MoS_2 nanosheets as catalysts for hydrogen evolution reaction. *Nano Lett.* **13,** 6222–6227 (2013).
23. Tsai, C., Abild-Pedersen, F. & Nørskov, J. K. Tuning the MoS_2 edge-site activity for hydrogen evolution via support interactions. *Nano Lett.* **14,** 1381–1387 (2014).
24. Li, Y. *et al*. MoS_2 nanoparticles grown on graphene: an advanced catalyst for the hydrogen evolution reaction. *J. Am. Chem. Soc.* **133,** 7296–7299 (2011).
25. Yang, J. *et al*. Two-dimensional hybrid nanosheets of tungsten disulfide and reduced graphene oxide as catalysts for enhanced hydrogen evolution. *Angew. Chem. Int. Ed.* **52,** 13751–13754 (2013).
26. Chen, J.-R. *et al*. Control of Schottky barriers in single layer MoS_2 transistors with ferromagnetic contacts. *Nano Lett.* **13,** 3106–3110 (2013).
27. Das, S., Chen, H.-Y., Penumatcha, A. V. & Appenzeller, J. High performance multilayer MoS_2 transistors with scandium contacts. *Nano Lett.* **13,** 100–105 (2013).
28. Yoon, Y., Ganapathi, K. & Salahuddin, S. How good can monolayer MoS_2 transistors be? *Nano Lett.* **11,** 3768–3773 (2011).
29. Popov, I., Seifert, G. & Tománek, D. Designing electrical contacts to MoS_2 monolayers: a computational study. *Phys. Rev. Lett.* **108,** 156802 (2012).
30. Liu, H., Neal, A. T. & Ye, P. D. Channel length scaling of MoS_2 MOSFETs. *ACS Nano* **6,** 8563–8569 (2012).
31. Liu, H. *et al*. Switching mechanism in single-layer molybdenum disulfide transistors: an insight into current flow across Schottky barriers. *ACS Nano* **8,** 1031–1038 (2014).
32. Kaushik, N. *et al*. Schottky barrier heights for Au and Pd contacts to MoS_2. *Appl. Phys. Lett.* **105,** 113505 (2014).
33. Liu, H. *et al*. Statistical study of deep submicron dual-gated field-effect transistors on monolayer chemical vapor deposition molybdenum disulfide films. *Nano Lett.* **13,** 2640–2646 (2013).
34. Allain, A., Kang, J., Banerjee, K. & Kis, A. Electrical contacts to two-dimensional semiconductors. *Nature Mater.* **14,** 1195–1205 (2015).
35. Kappera, R. *et al*. Phase-engineered low-resistance contacts for ultrathin MoS_2 transistors. *Nature Mater.* **13,** 1128–1134 (2014).
36. Kappera, R. *et al*. Metallic 1T phase source/drain electrodes for field effect transistors from chemical vapor deposited MoS_2. *APL Mater.* **2,** 092516 (2014).
37. Eda, G. *et al*. Coherent atomic and electronic heterostructures of single-layer MoS_2. *ACS Nano* **6,** 7311–7317 (2012).
38. Liao, L. *et al*. MoS_2 formed on mesoporous graphene as a highly active catalyst for hydrogen evolution. *Adv. Funct. Mater.* **23,** 5326–5333 (2013).
39. Chang, Y.-H. *et al*. Highly efficient electrocatalytic hydrogen production by MoS_x grown on graphene-protected 3D Ni foams. *Adv. Mater.* **25,** 756–760 (2013).
40. Conway, B. E. & Tilak, B. V. Interfacial processes involving electrocatalytic evolution and oxidation of H_2, and the role of chemisorbed H. *Electrochim. Acta* **22–23,** 3571–3594 (2002).
41. Li, H. *et al*. Activating and optimizing MoS_2 basal planes for hydrogen evolution through the formation of strained sulphur vacancies. *Nature Mater.* **15,** 48–53 (2016).
42. Komsa, H.-P. *et al*. Two-dimensional transition metal dichalcogenides under electron irradiation: defect production and doping. *Phys. Rev. Lett.* **109,** 035503 (2012).
43. Zhou, W. *et al*. Intrinsic structural defects in monolayer molybdenum disulfide. *Nano Lett.* **13,** 2615–2622 (2013).
44. Hong, J. *et al*. Exploring atomic defects in molybdenum disulphide monolayers. *Nature Commun.* **6,** 6293 (2015).
45. Qiu, H. *et al*. Hopping transport through defect-induced localized states in molybdenum disulphide. *Nature Commun.* **4,** 2642 (2013).
46. McDonnell, S., Addou, R., Buie, C., Wallace, R. M. & Hinkle, C. L. Defect-dominated doping and contact resistance in MoS_2. *ACS Nano* **8,** 2880–2888 (2014).
47. Tongay, S. *et al*. Defects activated photoluminescence in two-dimensional semiconductors: interplay between bound, charged, and free excitons. *Sci. Rep.* **3,** 2657 (2013).
48. Tran, P. D. *et al*. Coordination polymer structure and revisited hydrogen evolution catalytic mechanism for amorphous molybdenum sulfide. *Nature Mater.* **15,** 640–646 (2016).

Acknowledgements

M.C. and D.V. acknowledge financial support from NSF DGE 0903661 and ECCS 1128335. T.A. acknowledges financial assistance from NSF (CAREER CHE-1004218, DMR-0968937, NanoEHS-1134289, NSF-ACIF, and Special Creativity Grant).

C.d.C.C.e.S. acknowledges the Conselho Nacional de Desenvolvimento Científico e Tecnológico-Brazil, for a fellowship. J.Y. and M.C. acknowledge financial support from Rutgers Energy Institute. A.M. acknowledges LDRD program at LANL for funding this work. M.J.L. and P.E.B. acknowledge support from the US DOE, Office of Science, BES Award No. DE-SC0005132 and NSF No. 0959905. L.B., D.E., and V.B.S. acknowledge EFMA-542879, CMMI-1363203 and CBET-1235870 from the US National Science Foundation.

Author contributions

M.C. and D.V. conceived the idea and designed the experiments. D.V. performed the HER measurements and the physical characterizations of the samples. M.C. and D.V. analysed the data and wrote the manuscript. R.F. and R.K. fabricated the devices and helped D.V. with the contact resistance calculations. C.d.C.C.e.S. and J.Y. assisted D.V. with the HER measurements. D.K. and I.B. synthesized the single-layer MoS_2 nanosheets. M.J.L. and P.E.B. carried out the STEM measurements on MoS_2. L.D. and D.E. performed the DFT calculations. V.B.S. discussed the results of the DFT calculations with M.C. and D.V.; G.G., A.D.M. and T.A. discussed the results with M.C. and D.V.

Additional information

Supplementary information is available in the online version of the paper. Reprints and permissions information is available online at www.nature.com/reprints. Correspondence and requests for materials should be addressed to M.C.

Competing financial interests

The authors declare no competing financial interests.

Methods

Growth of CVD MoS_2. Single-layer MoS_2 nanosheets were grown by chemical vapour deposition (CVD) using MoO_3 and sulfur powder as precursors. 50 mg of MoO_3 and 250 mg of sulfur were placed in two alumina boats, respectively in the centre and upstream of the tube furnace. SiO_2/Si wafers were placed face-up on top of MoO_3. Air was evacuated by flowing Ar (Ultrahigh purity, Air Gas) for 15 min at 200 sccm. The tube was heated at 200 °C for 15 min to remove moisture from the precursors. Then the temperature was increased to 750° under a 90 sccm Ar flow. After 45 min, the furnace was cooled down to room temperature and the samples were removed from the furnace.

Device fabrication procedure. Edge-exposed and edge-covered MoS_2 electrochemical microcells were fabricated using CVD-grown single-layer (SL) MoS_2 nanosheets (Supplementary Fig. 2). As-grown SL MoS_2 nanosheets were transferred onto pre-patterned silicon substrates capped with a 300-nm oxide layer. The pre-patterned substrates consist of SiO_2/Si wafers on top of which 16 gold contact pads have been fabricated using a conventional photolithography process. We performed e-beam lithography to open microelectrode patterns connecting one MoS_2 nanosheet to one of the outside contact pads. The gold electrodes (80 nm) were deposited by means of e-beam evaporation at a deposition rate of 0.5 Å s^{-1} under high-vacuum conditions (10^{-7} torr). Each contact pad is connected to only one MoS_2 nanosheet, allowing each nanosheet to be tested separately. Once the MoS_2 nanosheets are contacted, we performed another e-beam lithography step to expose the MoS_2 nanosheet and cover the gold electrodes (passivation step).

Preparation of 1T-phase MoS_2 electrochemical microcells. The 2H-phase MoS_2 nanosheets were converted using *n*-butyllithium following the same protocol as reported earlier[35,49]. The microcells were first annealed at 95 °C under argon for 30 min to remove moisture from the surface of MoS_2. The wafers were then soaked in *n*-butyllithium (1.6 M in hexane, CAUTION: *n*-butyllithium is highly pyrophoric!) for 2–7 days in an argon-filled glove box. The samples were then washed with hexane and finally carefully rinsed with deionized water. Local conversion of 2H-phase MoS_2 to 1T phase was performed through treatment with *n*-butyllithium. Patterned conversion was done using a lithographic technique in which regions for conversion were treated whereas the other regions were protected by PMMA. For example, to make 1T-phase low-resistance contacts, the basal plane was covered whereas the MoS_2 contact regions were exposed to *n*-butyllithium. Further details can be found in the Supplementary Information.

Electrocatalytic measurements. The HER measurements were performed in a three-electrode configuration using a glassy carbon rod (Alfa Aesar) and a home-made Ag/AgCl microelectrode as counter and reference electrode, respectively. The gold contact pads connected to the MoS_2 were used as working electrode. The electrochemical measurements were carried out using a Multistat 1480 potentiostat from Solartron Group in a 0.5 M H_2SO_4 electrolyte solution. The polarization curves were obtained by sweeping the potential of the working electrode from 0 to −700 mV versus the reference electrode at a scan rate of 5 mV s^{-1}. The Ag/AgCl reference electrode was calibrated by using a RHE calibrated calomel electrode. In 0.5 M H_2SO_4, we measured:

$$E_{RHE} = E_{Ag/AgCl} + 218\,mV$$

The current measured from the working electrode was in the range 10^{-9}–10^{-6} A. The current density was calculated by normalizing the current to the total surface of MoS_2 exposed to the electrolyte solution. AC impedance spectroscopy was performed on the microcell at $\eta = 0.250$ V from 10^6 to 0.1 Hz with an alternating current voltage of 10 mV using a SI-1260 Impedance/Gain Phase analyser from Solartron Group.

HAADF-STEM of single-layer MoS_2. The high-angle annular dark-field scanning transmission electron microscopy (HAADF-STEM) imaging work was performed using a Nion UltraStem equipped with an aberration corrector, which allows us to obtain spatial resolution down to ∼1 Å at an operating voltage of 60 kV. The condenser lens system was set to produce an illumination probe semi-angle of 35 mrad and a beam current of ∼10–20 pA. To minimize the generation of beam-induced defects in the imaged regions we establish a simple two-step protocol: first, the initial inspection of MoS_2 flakes was conducted using a 1–2 µs dwell time, which represents the best compromise between structure visualization and damage prevention. Second, the adjustments of probe defocus and astigmatism were conducted on a region that is adjacent to the imaged area. Image processing was performed using a Gaussian filter with a full-width at half-maximum of 0.5 Å, which limits the measurement noise and not the structure.

References

49. Voiry, D. *et al*. Covalent functionalization of monolayered transition metal dichalcogenides by phase engineering. *Nature Chem.* **7,** 45–49 (2015).